Unfavorable Hip Stress Distribution After Legg–Calvé–Perthes Syndrome: A 25-Year Follow-Up of 135 Hips

Boštjan Kocjančič,[1] Andrej Moličnik,[2] Vane Antolič,[1] Blaž Mavčič,[1] Veronika Kralj-Iglič,[3] Rok Vengust[1]

[1]Department of Orthopaedic Surgery, University Medical Centre Ljubljana, Ljubljana, Slovenia, [2]Division of Surgery, University Medical Centre Maribor, Maribor, Slovenia, [3]Laboratory of Clinical Biophysics, Faculty of Health Sciences, University of Ljubljana, Zdravstvena 5, SI-1000 Ljubljana, Slovenia

Received 11 February 2013; accepted 8 August 2013
Published online 13 September 2013 in Wiley Online Library (wileyonlinelibrary.com). DOI 10.1002/jor.22479

ABSTRACT: To study the effect of hip and pelvis geometry on development of the hip after Perthes disease, we determined the resultant hip force and contact hip stress distribution in a population of 135 adult hips of patients who had been treated for Perthes disease in childhood. Contra-lateral hips with no record of disease were taken as the control population. Biomechanical parameters were determined by mathematical models for resultant hip force in one-legged stance and for contact hip stress, which use as an input the geometrical parameters assessed from anteroposterior radiographs. The mathematical model for stress was upgraded to account for the deviation of the femoral head shape from spherical. No differences were found in resultant hip force and in peak contact hip stress between the hips that were in childhood subject to Perthes disease and the control population, but a considerable (148%) and significant ($p < 0.001$) difference was found in the contact hip stress gradient index, expressing an unfavorable, steep decrease of contact stress at the lateral acetabular rim. This finding indicates an increased risk of early coxarthritis in hips subject to Perthes disease. © 2013 Orthopaedic Research Society. Published by Wiley Periodicals, Inc. J Orthop Res 32:8–16, 2014.

Keywords: Perthes disease; avascular necrosis; hip stress; microparticles; long term follow-up

Legg–Calvé–Perthes syndrome (Perthes disease) causes disturbances in development of the hip and pelvis. To compensate for the decreased ability of the hip to bear load, a femoral head with locally enlarged radius of the articular surface (coxa magna) is formed. The reason for the disease is still obscure, although avascular osteonecrosis is a possible etiological factor.[1–6] Early development of coxarthritis is considered a late consequence of Perthes disease.[4]

Biomechanical parameters have been determined from standard AP radiographs by using mathematical models that are simple enough to enable analysis of large patients populations.[7–9] The models within the HIPSTRESS method[7–9,11] previously proved useful in clinical evaluation of hip dyplasia,[10–12] slip of the femoral epiphysis,[13] avascular necrosis,[9,14] and coxarthritis,[15,16] and explained clinical outcomes of osteotomies.[17–19] These parameters could also be affected in hips subject to Perthes disease. Previous studies revealed peak contact stress as a relevant parameter for assessing increased risk of coxarthritis.[15,16,20] However, in cases where the resultant hip force and peak stress gave no answer, the effect of unfavorable stress distribution could be revealed by positive values of the index of hip stress gradient.[9,11,21]

To explore the origin of the early and late consequences of Perthes disease, we evaluated a population of hips subject to the disease using different clinical and biomechanical parameters at the time of the disease and after long-term follow-up, and compared this population with the normal contra-lateral hips with no record of disease. Based on previous evidence that a long lasting unfavorable hip stress distribution is related to early coxarthritis,[15,16] we sought well-defined objective indications whether hips subject to Perthes disease are at higher risk of early coxarthritis development.

In the stress model previously used in clinical studies[8,9] the shape of the articular surface was assumed spherical. Coxa magna notably deviates from a spherical shape; therefore, we upgraded the model to assume deviations from a spherical shape.

MATERIALS AND METHODS

Patients and Hips

Two hundred fifty-nine patients were treated for Perthes disease between January 1975 and December 1995. In 2010, 167 of these patients (64.5%) attended a control examination that included measurement of their height and weight. We omitted 3 patients whose earlier radiographs could not be found, 19 patients with bilateral disease, 3 patients for whom follow-up radiographs had not been taken, 5 patients due to deficient radiograph quality, and 2 patients who had undergone a hip replacement due to coxarthritis. The remaining 135 (24 females, 111 males) agreed to participate (Table 1). Forty-three hips (31.9%) had been treated conservatively and 92 hips (68.1%) operatively. Of these, 1 hip underwent osteotomy of the greater trochanter, 85 underwent intertrochanteric osteotomy, and 6 underwent pelvic osteotomy. The average age at first hospital admission was 6.9 (2.4 to 17.6) years; 6.23 (2.4–17.6) years for conservatively treated patients and 7.2 (3.6–15.2) years for operatively treated patients. The average age at operation was 7.6 (3.7–15.2) years. The average age at follow-up was 32.5 (20.6–47.6) years. BMI at follow up was 26.7 (18–38) kg/m^2. The time interval between treatment and follow-up was 25.6 (14.5–34.5) years; 23.9 (15.9–32.8) for conservatively treated patients and 26.4 (14.5–34.5) years for operatively treated patients. Radiographs with the lateral view of the femoral head for both hips were available for 111 patients.

The authors declare that they have no conflicts of interest regarding to this work.
Grant sponsor: Slovenian Research Agency; Grant number: J3-4108.
Correspondence to: Veronika Kralj-Iglič (T: +386-41720766; F: +38613001119; E-mail: veronika.kralj-iglic@fe.uni-lj.si)

Table 1. Distribution of Patients Subject to Perthes Disease With Respect to Sex, Clinical Scores, and Treatment (Conservative or Operative)

	Conservatively Treated	Operatively Treated
Number of patients	43	92
Male	35	75
Female	8	17
Caterall 1	7	13
Caterall 2	22	34
Caterall 3	8	37
Caterall 4	6	8
Herring A	9	9
Herring B	23	36
Herring C	11	47
Stulberg 1	2	1
Stulberg 2	27	30
Stulberg 3	11	50
Stulberg 4	2	8
Stulberg 5	1	3

Clinical and Radiographic Evaluation

Hips subject to Perthes disease were classified according to the Catterall grouping[22] and the Herring lateral pillar classification,[23] At follow-up, radiographs were classified into five groups as proposed by Stulberg et al.[24] The presence of arthritis at follow-up was assessed using the Kellgren and Lawrence classification.[25] Clinical outcome was evaluated by the Harris Hip Score (HHS)[26] and by the WOMAC,[27] Clinical scores were assessed by two independent experienced surgeons. The intraclass correlation coefficients were: 0.931 for Caterall score, 0.889 for Herring lateral pillar score and 0.754 for Stulberg score with kappa agreements of 0.83, 0.83, and 0.5, respectively, comparable with previously published results.[28]

Biomechanical Evaluation

Biomechanical parameters at follow-up were determined using 3D models. The cartilage was described as an elastic continuum.[29] The resultant hip force $\mathbf{R}$ was calculated in one–legged stance.[7] The model was individualized by accounting for the patient's muscle attachment points according to parameters obtained from the standard AP radiograph (inter-hip distance (l), height (H), and width (C) of the pelvis, and the position of the effective muscle attachment on the greater trochanter relative to the head center (x,z)).[7] Radiographic magnification was calibrated by including a 32 mm ball placed between the legs. Deviation from a spherical head was estimated by measuring the radius of curvature of the loaded femoral head from frontal and lateral views (r_f and r_l, respectively).

Contact stress distribution represented by the peak stress on the load bearing area (p_{max}), position of the stress pole (Θ), index of the stress gradient at the lateral acetabular rim (G_p), functional load bearing angle ϑ_f and load bearing area A_f, were calculated by using a 3D model of the articular surface[9] adapted with respect to deviations of the head shape from spherical. The head was defined within the intrinsic coordinate system (x',y',z'), while the acetabulum was defined within the coordinate system (x,y,z) (Fig. 1). When loaded, the origin of the head system is displaced with respect to that of the acetabulum by a small distance d (Fig. 1) causing some head points to approach the acetabulum and some to move away. The stress pole was the point at which the head and the acetabulum were closest. In the one-legged stance, the resultant hip force was found to lay in the frontal plane,[7] so the pole also lies in this plane. The radius vector to the pole points in the direction of the displacement. A point is chosen on the femoral surface. The magnitudes of the radius vectors from the origins of both coordinate systems to this point (r and r', respectively) are connected by a trigonometric relation:

$$r^2 = r'^2 + d^2 - 2rd\cos\gamma \tag{1}$$

where γ is the space angle in the acetabular system (Fig. 1). The cosine of γ is:

$$\cos\gamma = \frac{\mathbf{r}_p \cdot \mathbf{r}}{|\mathbf{r}_p||\mathbf{r}|} \tag{2}$$

where $\mathbf{r}_p$ is the radius vector to the pole in the acetabular system, $\mathbf{r}$ is the radius vector to the chosen point on the acetabular shell, while $|\mathbf{r}_p|$ and $|\mathbf{r}|$ are the respective magnitudes of these vectors. d was assumed small with respect to $|\mathbf{r}_p|$ and $|\mathbf{r}|$ so that γ is the same in the displaced system of the femoral head

$$\cos\gamma = \frac{\mathbf{r}'_p \cdot \mathbf{r}'}{|\mathbf{r}'_p||\mathbf{r}'|} \tag{3}$$

Stress p is assumed proportional to the difference $|\mathbf{r}_p| - |\mathbf{r}|$. Considering Equation (1) and a small d,[29]

$$p \propto (|\mathbf{r}_p| - |\mathbf{r}|) = d\cos\gamma \tag{4}$$

The femoral head surface is described by a vector

$$\mathbf{r} = r\left(\cos\varphi\sin\vartheta, \left(1 - \frac{\delta}{r}\right)\sin\varphi, \cos\varphi\cos\vartheta\right) \tag{5}$$

and the stress pole is given by a vector

$$\mathbf{r}_p = r(\cos\Phi\sin\Theta, \sin\Phi, \cos\Phi\cos\Theta) \tag{6}$$

For convenience, the coordinate system is rotated and the pole lies in the direction of the z-axis, so $\sin\Phi = 0$ and $\cos\Theta = 1$,

$$\mathbf{r}_p = r(0, 0, 1) \tag{7}$$

Equations (5) and (6) yield:

$$\mathbf{r}_p \cdot \mathbf{r} = r^2\cos\varphi\cos\vartheta \tag{8}$$

while the vector magnitudes are:

$$|\mathbf{r}_p| = r \tag{9}$$

$$|\mathbf{r}| = r\left(1 - \frac{\delta}{r}\sin^2\varphi\right) \tag{10}$$

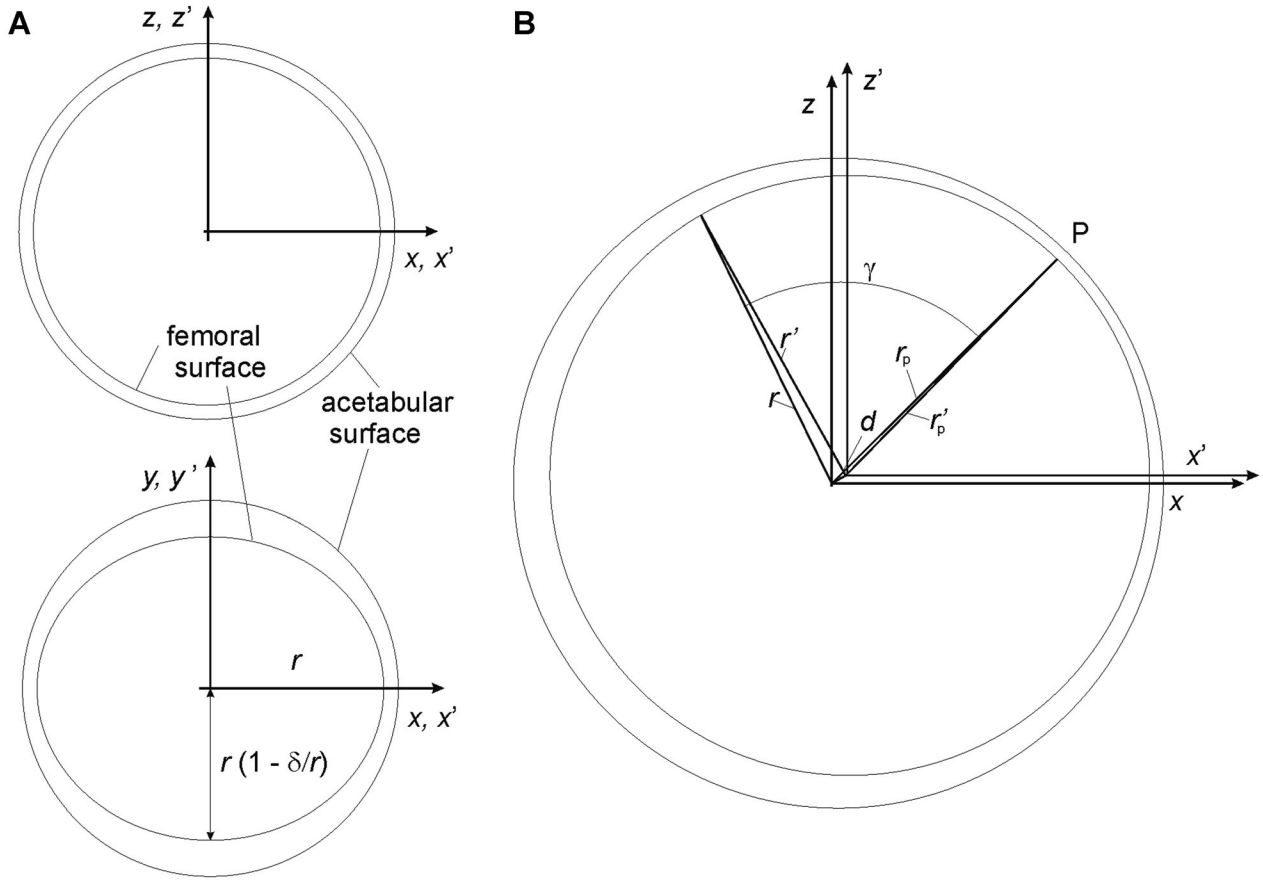

Figure 1. Scheme of the unloaded (A) and loaded (B) hip. When unloaded, the femoral and the acetabular surfaces are concentric; when loaded, the femoral surface and its intrinsic coordinate system are displaced in the direction of the stress pole in the frontal plane (P). The acetabular surface is spherical, while the femoral surface is axisymmetric with respect to the x-axis.

The cosine of γ is:

$$\cos\gamma = \cos\varphi\cos\vartheta\left(1+\frac{\delta}{r}\sin^2\varphi\right) \tag{11}$$

so that the stress is expressed by

$$p = p_0\cos\varphi\cos\vartheta\left(1+\frac{\delta}{r}\sin^2\varphi\right) \tag{12}$$

To obtain the expression for the area element vector, the derivatives with respect to the angles are calculated:

$$\boldsymbol{r}_\varphi = r\left(-\sin\varphi\sin\vartheta, \left(1-\frac{\delta}{r}\right)\cos\varphi, -\sin\varphi\cos\vartheta\right) \tag{13}$$

$$\boldsymbol{r}_\vartheta = r(\cos\varphi\cos\vartheta, 0, -\cos\varphi\sin\vartheta) \tag{14}$$

so that the elements of the 1st form are:

$$E = \boldsymbol{r}_\varphi\cdot\boldsymbol{r}_\varphi = r^2\left(1-2\frac{\delta}{r}\cos^2\varphi\right) \tag{15}$$

$$F = \boldsymbol{r}_\varphi\cdot\boldsymbol{r}_\vartheta = 0 \tag{16}$$

$$G = \boldsymbol{r}_\vartheta\cdot\boldsymbol{r}_\vartheta = r^2\cos^2\varphi \tag{17}$$

The magnitude of the area element is:

$$\mathrm{d}A = \sqrt{EG-F^2}\,\mathrm{d}\varphi\,\mathrm{d}\vartheta = r^2\left(1-\frac{\delta}{r}\cos^2\varphi\right)\cos\varphi\,\mathrm{d}\varphi\,\mathrm{d}\vartheta \tag{18}$$

while the area element vector is:

$$\begin{aligned}\mathrm{d}\mathbf{A} = (\mathrm{d}A_x, \mathrm{d}A_y, \mathrm{d}A_z) = r^2\left(1-\frac{\delta}{r}\cos^2\varphi\right)\times\\ \cos\varphi\,\mathrm{d}\varphi\,\mathrm{d}\vartheta\left(\cos\varphi\sin\vartheta, \left(1-\frac{\delta}{r}\right)\sin\varphi, \cos\varphi\cos\vartheta\right)\end{aligned} \tag{19}$$

Integration of stress over the load bearing area gives the resultant hip joint force,

$$\int p\,\mathrm{d}\boldsymbol{A} = \mathbf{R} \tag{20}$$

The load bearing area is in the rotated system determined within the intervals $\varphi\in[-\pi/2,\ \pi/2]$ and $\vartheta\in[-\pi/2,\ \vartheta_{\mathrm{CE}}-\Theta]$, where ϑ_{CE} is the Wiberg center-edge angle defined by the lateral acetabular rim.[9] Using Equations (12), (19) and (20)

yields:

$$\int p\mathrm{d}A_x = p_0 r^2 \int_{-\pi/2}^{\pi/2} \cos^3\varphi\left(1+\frac{\delta}{r}\sin^2\varphi\right)\left(1-\frac{\delta}{r}\cos^2\varphi\right)\mathrm{d}\varphi\times \int_{-\pi/2}^{\vartheta_{\mathrm{CE}}-\Theta} \sin\vartheta\cos\vartheta\,\mathrm{d}\vartheta = R_x \tag{21}$$

$$\int p\mathrm{d}A_y = p_0 r^2\left(1-\frac{\delta}{r}\right)\int_{-\pi/2}^{\pi/2} \cos^2\varphi\sin\varphi\left(1+\frac{\delta}{r}\sin^2\varphi\right)\left(1-\frac{\delta}{r}\cos^2\varphi\right)\mathrm{d}\varphi\times \int_{-\pi/2}^{\vartheta_{\mathrm{CE}}-\Theta} \cos\vartheta\,\mathrm{d}\vartheta = 0 \tag{22}$$

$$\int p\mathrm{d}A_z = p_0 r^2 \int_{-\pi/2}^{\pi/2} \cos^3\varphi\left(1+\frac{\delta}{r}\sin^2\varphi\right)\left(1-\frac{\delta}{r}\cos^2\varphi\right)\mathrm{d}\varphi\times \int_{-\pi/2}^{\vartheta_{\mathrm{CE}}-\Theta} \cos^2\vartheta\,\mathrm{d}\vartheta = R_z \tag{23}$$

where in the rotated system.[9]

$$\mathbf{R} = (R_x, R_y, R_z) = R(\sin(\vartheta_R+\Theta), 0, \cos(\vartheta_R+\Theta)) \tag{24}$$

Evaluating the integrals in (21) and (23) gives:

$$R\sin(\vartheta_R+\Theta) = -\frac{2}{3}p_0 \mathrm{r}^2\left(1-\frac{3}{5}\frac{\delta}{r}\right)\cos^2(\vartheta_{\mathrm{CE}}-\Theta) \tag{25}$$

$$R\cos(\vartheta_R+\Theta) = -\frac{2}{3}p_0 \mathrm{r}^2\left(1-\frac{3}{5}\frac{\delta}{r}\right)\left(\frac{\pi}{2}+\vartheta_{\mathrm{CE}}-\Theta+\frac{1}{2}\sin\left(2(\vartheta_{\mathrm{CE}}-\Theta)\right)\right) \tag{26}$$

where R is the magnitude of the resultant hip force and ϑ_R is the inclination of resultant hip force with respect to the vertical.[7]

Dividing Equation (25) by Equation (26) recovers a nonlinear equation for the coordinate of the pole Θ[8,9]:

$$\tan(\vartheta_R+\Theta) = \frac{\cos^2(\vartheta_{\mathrm{CE}}-\Theta)}{\left(\frac{\pi}{2}+\vartheta_{\mathrm{CE}}-\Theta+\frac{1}{2}\sin\left(2(\vartheta_{\mathrm{CE}}-\Theta)\right)\right)} \tag{27}$$

while p_0 can then be expressed from Equation (25):

$$p_0 = \frac{3R}{2r^2}\frac{\sin(\vartheta_R+\Theta)}{\cos^2(\vartheta_{\mathrm{CE}}-\Theta)\left(1-\frac{3}{5}\frac{\delta}{r}\right)} \tag{28}$$

or, by considering that δ/r is small:

$$p_0 = p_{0,\mathrm{sph}}\left(1+\frac{3}{5}\frac{\delta}{r}\right) \tag{29}$$

where "sph" denotes the corresponding result of the model with a spherical head[8,9]:

$$p_{0,\mathrm{sph}} = \frac{3R}{2r^2}\frac{\sin(\vartheta_R+\Theta)}{\cos^2(\vartheta_{\mathrm{CE}}-\Theta)} \tag{30}$$

Accordingly,

$$p_{\max} = p_{\max,\mathrm{sph}}\left(1+\frac{3}{5}\frac{\delta}{r}\right) \tag{31}$$

The stress gradient is expressed in spherical coordinates:

$$\nabla p = \left(\frac{\partial p}{\partial r}, \frac{1}{r}\frac{\partial p}{\partial \vartheta}, \frac{1}{r\sin\vartheta}\frac{\partial p}{\partial \varphi}\right) \tag{32}$$

It follows from Equations (12) and (32) that:

$$\nabla p = \left(0, -\frac{p_0}{r}\sin\vartheta\left(1+\frac{\delta}{r}\sin^2\varphi\right)\cos\varphi, -\frac{p_0}{r}\cot\vartheta\sin\varphi\left(1+\frac{\delta}{r}(\sin^2\varphi-2\cos^2\varphi)\right)\right) \tag{33}$$

Since the resultant force lies in the frontal plane,[7] the problem was mapped into 2D. The hip stress gradient index was defined as the gradient magnitude at the lateral acetabular rim ($\vartheta = \vartheta_{\mathrm{CE}} - \Theta$) while the angle Θ was considered as an ordinary angle and not a spherical coordinate. Θ was positive in the lateral direction from the radius vector to the stress pole and negative in the medial direction.[9,11] The hip stress gradient index is the magnitude of the gradient at $\vartheta = \vartheta_{\mathrm{CE}} - \Theta$ and $\varphi = 0$,

$$G_p = -\frac{p_0}{r}\sin(\vartheta_{\mathrm{CE}}-\Theta) = G_{p,\mathrm{sph}} \tag{34}$$

which is the same as in the case of a spherical head.[9,11] If the pole of stress distribution lies outside the load bearing area (i.e., $\Theta > \vartheta_{\mathrm{CE}}$) then $G_p > 0$; if it lies inside the weight bearing area (i.e., $\Theta < \vartheta_{\mathrm{CE}}$) then $G_p < 0$ (Fig. 2). A positive hip stress gradient index pertains to unfavorable stress distribution that decreases medially. In these hips, the load bearing area is smaller.

The load bearing area is (Equation 18)

$$A = \int_{-\pi/2}^{\pi/2} r^2\left(1-\frac{\delta}{r}\cos^2\varphi\right)\cos\varphi\,\mathrm{d}\varphi\times \int_{-\pi/2}^{\vartheta_{\mathrm{CE}}-\Theta}\mathrm{d}\vartheta = 2r^2\left(\frac{\pi}{2}+\vartheta_{\mathrm{CE}}-\Theta\right)\left(1-\frac{4}{3}\frac{\delta}{r}\right) \tag{35}$$

or

$$A = A_{\mathrm{sph}}\left(1-\frac{4}{3}\frac{\delta}{r}\right) \tag{36}$$

where

$$A_{\mathrm{sph}} = 2r^2\left(\frac{\pi}{2}+\vartheta_{\mathrm{CE}}-\Theta\right) \tag{37}$$

The input data for stress were the magnitude and direction of the resultant hip force, the lateral coverage of the head by the acetabulum (the center-edge angle, ϑ_{CE}) and the curvature radii of the head contours in frontal and lateral views ($r_{\mathrm{f}} = r$ and $r_{\mathrm{l}} = r - \delta$, respectively). To assess head size, we used the effective radius:

$$r_{\mathrm{eff}} = \frac{(r_{\mathrm{f}}+r_{\mathrm{l}})}{2} = r\left(1-\frac{\delta}{2r}\right) \tag{38}$$

R, $p_{\max}$, and G_p are proportional to body weight; thus, we studied the normalized parameters (R/W_{B}, $p_{\max}/W_{\mathrm{B}}$, G_p/W_{B}) that reveal the impact of the hip and pelvis geometry.

Statistical Methods

Methods of descriptive statistics were used to determine differences between test and control populations and correlations between clinical, radiographic, biomechanical, and

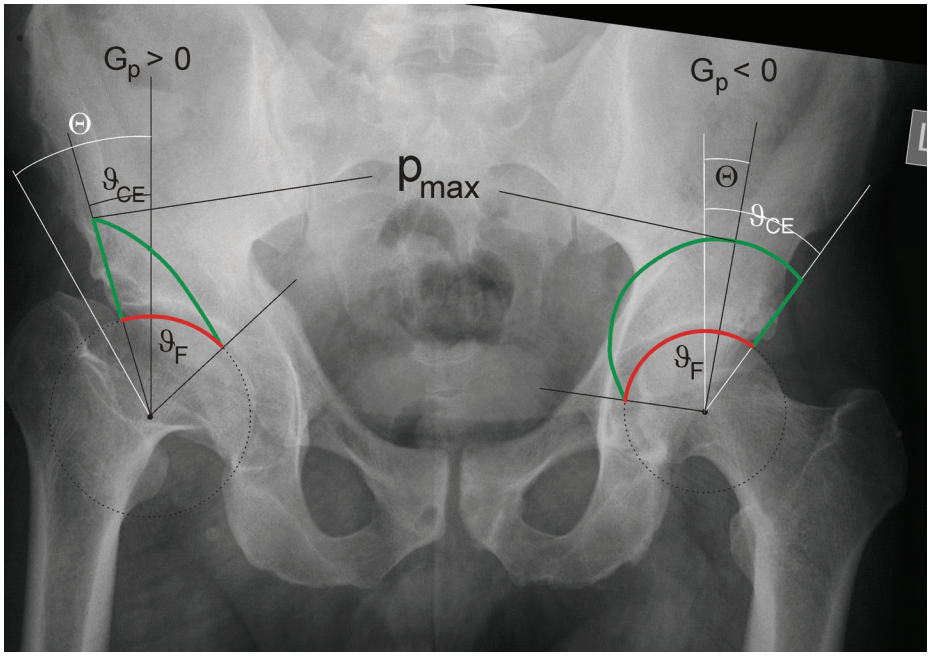

Figure 2. Hip stress distribution in a hip subject to Perthes disease in childhood (right hip) and a normal hip stress distribution (left hip). The green lines above the articular sphere denote the magnitude of stress in the frontal plane through the center of the articular sphere of both hips. In the deformed hip, the stress pole lies outside the load bearing area, and the functional angle is small. Stress decreases monotonously in the medial direction and the hip stress gradient index is positive. In the healthy hip, the pole lies within the load bearing area, and the functional angle is large, enabling a larger portion of the head to bear load. At the lateral rim, stress increases medially, reaches a maximum and then decreases; thus, the hip stress gradient index is negative. Peak stress is nevertheless almost equal in both hips due to the larger radius of the articular surface in the diseased hip.

geometrical parameters. We used the paired *t*-test and the Pearson correlation coefficient (ρ), with the respective probabilities (p) expressing significance. Average values (and Std Dev), probabilities, and Pearson coefficients were calculated with Microsoft® Office Excel® 2007 SP3. The probabilities of correlations were calculated with *p*-value Calculator for Correlation Coefficients: http://www.danielsoper.com/statcalc3/calc.aspx?id=44. Statistical power was calculated with the Power & Sample Size Calculator: http://www.statistical-solutions.net/pss_calc.php.

The impact of biomechanical/radiographic parameters on HHS was tested on the subgroup of non-operatively treated male hips by multiple linear regression models in which HHS was the dependent variable. The patients' age and BMI were covariates, while the biomechanical/radiographic parameters were separately entered as independent predictors. For each independent predictor, results were reported in terms of the adjusted ρ^2 value for the entire model, the predictor-specific standardized β coefficient and p-value. In multiple regression models, the standardized β coefficient represents the change in the dependent variable (in terms of standard deviations) due to the change of the independent variable (in terms of standard deviation of this variable). Multivariate statistical analyses were performed with SPSS Statistics 17.0 for Windows (SPSS, Inc., Chicago, IL).

RESULTS

The relations between different clinical and radiographical parameters at follow-up confirmed that the data on the status of the hip were consistently related (Table 2). At follow-up, the average HHS was 89.8 ± 11 (94.4 (76–100) for conservatively treated patients and 87.6 (56–100) for operatively treated patients), the average WOMAC score was 6.7 ± 12 (0–68) and the average total range of motion was 229° (80–300°) for conservatively treated and 197° (60–290°) for operated patients. Significant bivariate correlations were found between the clinical evaluation at the time of the disease (Herring, Caterall) and the clinical evaluation at follow-up expressed by HHS (but not WOMAC) and between the clinical evaluation at the time of the

Table 2. Bivariate Correlations Between Clinical, Radiographic, and Biomechanical Scores in a Population of Hips Developed After Perthes Disease

ρ (p)	Caterall	Herring	Stulberg	Kelgreen	HHS	WOMAC
HHS	−0.23 (0.008)	$-0.28\ (10^{-3})$	$-0.40\ (2.10^{-6})$	$-0.30\ (4.10^{-4})$		
WOMAC	0.03 (0.80)	0.13 (0.14)	$0.27\ (2.10^{-3})$	0.24 (0.006)	$-0.64\ (<10^{-7})$	
G_p/W_B (m^{-3})	0.16 (0.06)	0.21 (0.014)	$0.43\ (2.10^{-7})$	0.26 (0.002)	−0.20 (0.02)	0.14 (0.12)

Pearson correlation coefficients (ρ) and corresponding probabilities (p) were calculated with a two-tailed distribution.

disease (Herring) and the contact hip stress gradient index G_p. Higher HHS and lower WOMAC scores corresponded to higher Kelgreen–Lawrence and higher Stulberg scores, indicating that HHS better reflects the relevant data for hips after Perthes disease than WOMAC, and proving G_p to be a relevant biomechanical parameter. The HHS was analyzed as the dependent variable by multiple linear regression models adjusted for age and BMI and considering the subgroup of non-operatively treated male hips ($n = 34$). Significant independent predictors included the Herring lateral pillar score (adjusted $\rho^2 = 0.16$, standardized $\beta = -0.46$, $p = 0.01$) and G_p (adjusted $\rho^2 = 0.08$, standardized $\beta = -0.36$, $p = 0.04$), while the Caterall score, the resultant hip force and the peak contact hip stress did not show significant correlations.

We found a considerable, significant difference in center-edge angle and in effective radius of the articular surface between the test and the control populations (Table 3). Hips subject to Perthes disease had poorer lateral coverage by the acetabulum, but a larger head ($\rho = -0.65$, $p < 0.001$, Fig. 3). No healthy hip had an angle $<18^\circ$ and an effective head radius >32 mm. Conversely, the data for hips subject to Perthes disease extended into the region of healthy hips, so many hips subject to Perthes disease developed a normal angle and a normal head.

Poor lateral head coverage increased the contact hip stress and the stress gradient index, while an articular sphere with a large effective radius decreased the contact hip stress and the gradient index. Opposing effects resulted in no significant difference in contact hip stress (Table 3), but the stress gradient and the position of the stress pole were less favorable in the test group (Table 3), the pole laying significantly more laterally (Table 3) resulting in a steeper stress distribution over the load bearing area. Accordingly, the angle that spanned this area was significantly smaller in the test group. However, because of the larger effective radius of the articular surface, the load-bearing area A_f was not different (with indecisive power $1 - \beta = 0.63$).

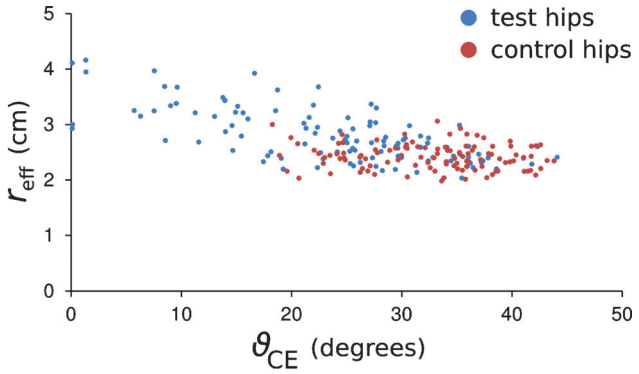

Figure 3. Effective radius of the head $r_{eff} = (r_f + r_l)/2$ as a function of the center-edge angle (ϑ_{CE}). Blue dots: hips subject to Perthes disease; red dots: contra-lateral healthy hips.

Both populations had the same dependence (albeit in different regions) of hip stress gradient index on the effective radius of the articular surface (A) and on the center-edge angle (B), indicating that the underlying mechanism is the same for all hips (Fig. 4). A majority

Table 3. Comparison Between Biomechanical Parameters Pertaining to Hips Developed After Perthes Disease (Test) and Control (Contra-Lateral) Hips

Average ± Std Dev	Test	Control	Approximated Difference (%)	Number of Hips, N	p	Power $(1-\beta)$
Center-edge angle, ϑ_{CE} (°)	24.1 ± 9.7	32.9 ± 6.5	−31	135	$<10^{-8}$	1.00
Average effective radius of the femoral head, r_{eff} (cm)	2.79 ± 0.48	2.41 ± 0.23	15	111	$<10^{-8}$	1.00
Resultant hip force, $R(N)$	2,099 ± 474	2,100 ± 472	0	135	0.936	$<10^{-3}$
Resultant hip force normalized by body weight, R/W_B	2.59 ± 0.23	2.59 ± 0.20	0	135	0.797	$<10^{-3}$
Peak stress on the load bearing area, p_{max} (MPa)	2.32 ± 0.81	2.30 ± 0.63	0	111	0.900	$<10^{-3}$
Peak stress on the load bearing area normalized by body weight, p_{max}/W_B (m^{-2})	2,940 ± 885	2,946 ± 793	0	111	0.949	$<10^{-3}$
Hip stress gradient index, G_p (MPa/m)	4.46 ± 43.55	−29.45 ± 29.69	>100	135	$<10^{-8}$	1.00
Hip stress gradient index normalized by body weight, G_p/W_B (m^{-3})	4,334 ± 51,011	−37,959 ± 35,848	>100	135	$<10^{-8}$	1.00
Load bearing area, A_f (cm^2)	23.3 ± 6.0	22.0 ± 4.6	6	111	0.08	0.63
Functional angle of the load bearing, ϑ_f (°)	90.2 ± 22.7	108.7 ± 13.5	−18	135	$<10^{-8}$	1.00
Position of the stress pole, Θ (°)	24.3 ± 13.9	13.9 ± 7.0	55	135	$<10^{-8}$	1.00

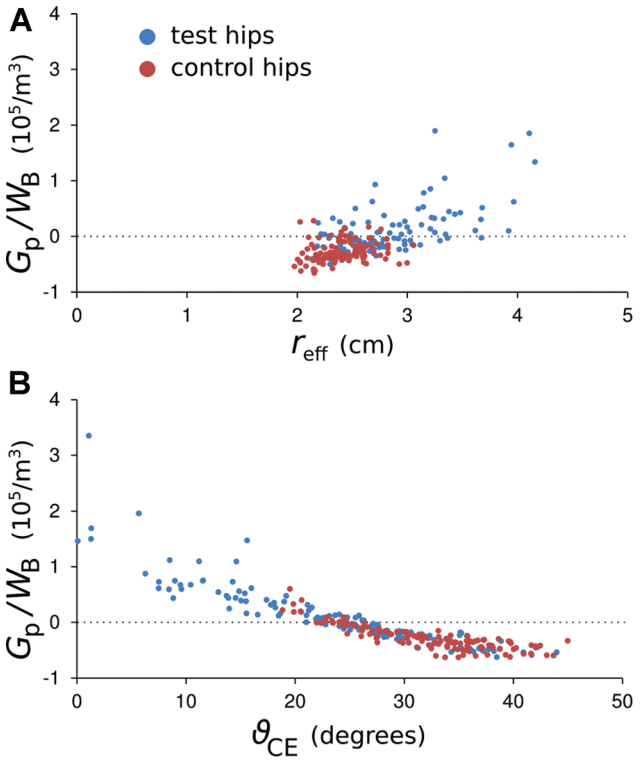

Figure 4. (A) Stress gradient index normalized by body weight (G_p/W_B) as a function of the effective head radius $r_{eff}=(r_f+r_l)/2$. (B) G_p/W_B as a function of center-edge angle (ϑ_{CE}). Blue dots: hips subject to Perthes disease; red dots: contra-lateral healthy hips.

of healthy hips had a negative G_p, while many hips with Perthes disease had a positive G_p. The correlation coefficients for the $G_p(r)$ and $G_p(\vartheta_{CE})$ dependences were -0.58 and 0.95, respectively ($p<0.001$).

DISCUSSION

The high HHS indicated a good outcome in hips subject to Perthes disease in childhood. The follow-up time (avg. 25 years) represents a lesser part of the patients' expected lifetimes, so this does not prove that hips with Perthes are equivalent to healthy hips. We therefore explored whether hips with Perthes were at risk of developing coxarthritis sooner than normal hips. We were interested in non-specific biomechanical parameters, so we included all hips as a single group, regardless of how they were treated (operatively or conservatively).

Hips with Perthes disease had smaller center-edge angles (Table 3, Fig. 3), which would increase peak stress. However, they had larger effective radii of the articular surface at load bearing, which would decrease peak stress. The two effects canceled each other, so no difference existed in peak stress between Perthes and healthy hips. However, hips with Perthes disease had a less favorable (steeper) distribution of contact stress over the load bearing area, reflected in the more lateral position of the stress pole, a larger stress gradient index, and a smaller span of the load bearing area. Because the gradient index, not the peak contact stress or the resultant hip force, was related to the disease, we believe stress distribution is important in hip development.[9,11,21]

Hips with coxa magna have flattened head under the lateral part of the acetabulum with poor lateral coverage. The model for such hips yielded a small functional angle of load bearing with steeply falling stress in the medial direction (Fig. 2). The surface was constructed solely based on the curvature of the part that bears load. Other parts of the head do not lie on the articular surface, but this is immaterial in the model since they are not subject to stress. In Perthes, substantial head deformity may be present.[30] In our population the surface deviated from a sphere. In 3 Perthes hips out of 111 the deviation (δ/r) was >20%, and in 6 it was between 10 and 20%. However, the effect on peak stress within both populations (test and control) was <3% (which is smaller than the effect of the estimated error of the assessment method).

In a study of 47 dysplastic and 36 healthy hips, Mavčič et al.[12] showed that peak contact stress was significantly higher in dysplastic hips. Articular surface radii were larger (by ~12%, compared to 15% in our study) in dysplastic hips. Another study found that the stress gradient index G_p was also significantly higher in dysplastic hips.[11] Based on these results, it cannot be concluded which parameter is decisive for assessing the risk of early coxarthritis. Here, we report the difference in G_p but not peak stress of hips with Perthes disease compared to control hips.

Multivariate analysis showed that the connection of the Herring lateral pillar score at the time of the disease and the follow-up G_p on the clinical status (HHS) of the hip was significant, but small, suggesting that after the appearance of symptoms, the disease progression is guided by several factors, with G_p (a biomechanical factor) and concomitant radiographic changes in the lateral pillar (morphological consequence of biomechanical factors) showing prominence. The significance of the impact of G_p and other biomechanical factors is marred by insufficiencies in the model, the limitations in imaging, and limited repeatability and accuracy of the method. Further, various radiographic classifications had poor inter-observer agreements/reliability.[31–33] Thus, the impact of the biomechanical factor in our analysis is underestimated.

The control hips were contralateral to hips with Perthes disease. As Perthes may occur bilaterally[6,34] our control group only approximates a group of healthy hips. The relevance of such an approximation is supported by the fact that hips matured after the onset (and treatment) of the disease and that Perthes disease or avascular necrosis of the head did not occur in contralateral hips. The contralateral hips' average radius and center-edge angle were comparable to those of normal hips. In a study of dysplastic hips[12]

the control group consisted of hips obtained from radiographs taken for reasons other than hip diseases (e.g., back pain). The average ϑ_{CE} was $31 \pm 6°$[12] which is close to our result of $32.9 \pm 6.5°$ (Table 3). The effective radius of the articular sphere of our control group was 24.1 ± 2.3 mm, close to the value 23 ± 10 mm found in the group of healthy hips.[12] However, in our study the population was mostly males with larger heads[35] whereas the healthy hips of the previous study[12] were all female.

Biomechanical analysis enables additional insight into mechanisms leading to avascular osteonecrosis. A study of adult hips with avascular necrosis was the first to point to the stress gradient as the relevant parameter.[9] The stress gradient index and not the peak contact hip stress or the resultant hip force differed significantly from the respective values for the control population. Hips with avascular necrosis were connected with an unfavorable (steep) distribution of contact stress, suggesting that a high stress gradient is an etiological factor for avascular necrosis.[9] Avascular necrosis has also been connected to corticosteroid therapy,[36] trauma, arterial disease, connective tissue disease (rheumatoid arthritis and systemic lupus erythematosus), sickle cell disease, alcoholism, Gaucher's disease,[37] disseminated intravascular coagulation,[38] intraosseous malignancy (especially lymphoma),[39] and HIV.[40] A common feature of these conditions is an increased concentration of microvesicles in isolates from peripheral blood.[41–52] Platelet-derived microvesicles carry tissue factor and may expose negatively charged phosphatidylserine on their exterior, so they are prothrombogenic and may cause formation of clots in blood vessels.[53] Microvesiculation can also be promoted by activation of platelets in shear flow. During motion, stress distribution changes over the load bearing area may cause shear stresses within the bones and their blood vessels. These stresses are larger when the stress gradient is large and its distribution strongly changes over a small area. High shear stress within deformed blood vessels causes increased microvesiculation of cells, especially platelets, and leads to formation of microemboli which hinder blood flow within the bones. Treatment of the disorder could be supported by substances that suppress microvesiculation and prevented by altering biophysical properties of blood. Heparin was suggested as a possible candidate.[54]

In juvenile osteonecrosis, altered stress distributions may cause disturbances in growth of affected bones growth leading to deformity of the hip and pelvis in adulthood. Femoral head deformities usually present as non-spherical with a short neck and large greater trochanter. In such hips, undesirable contact between the acetabular rim and the neck (femoroacetabular impingement) related to Perthes disease may be caused by the disease itself or as a consequence of its treatment[55] and may lead to early osteoarthritis and poor long-term outcomes.[56–58]

ACKNOWLEDGMENTS

The authors acknowledge support from the Slovenian Research Agency (grant J3-4108), and are indebted to Jasmina Jelovšek for assessment of geometrical parameters from anteroposterior radiographs.

REFERENCES

1. Kim HK. 2012. Pathophysiology and new strategies for the treatment of Legg-Calve-Perthes disease. J Bone Joint Surg Am 94:659–669.
2. Koob TJ, Pringle D, Gedbaw E, et al. 2007. Biomechanical properties of bone and cartilage in growing femoral head following ischemic osteonecrosis. J Orthop Res 25:750–757.
3. Sharma S, Shewale S, Sibinski M, et al. 2009. Legg-Calve-Perthes disease affecting children less than eight years of age: a paired outcome study. Int Orthop 33:231–235.
4. Kotilingam D, Sherlock D, Rosenstein A. 2011. Treatment options for symptomatic degenerative joint disease secondary to Legg-Calve-Perthes disease. Am J Orthop 40:E10–E13.
5. Herring JA. 1994. The treatment of Legg-Calve-Perthes disease. A critical review of the literature. J Bone Joint Surg Am 76:448–458.
6. Catterall A. 1984. Thoughts on the etiology of Perthes' disease. Iowa Orthop J 4:34–36.
7. Iglič A, Srakar F, Antolič V. 1993. The influence of the pelvic shape on the biomechanical status of the hip. Clin Biomech 8:223–224.
8. Ipavec M, Brand RA, Pedersen DR, et al. 1999. Mathematical modelling of stress in the hip during gait. J Biomech 32:1229–1235.
9. Kralj-Iglič V, Dolinar D, Ivanovski M, et al. 2012. Role of biomechanical parameters in hip osteoarthritis and avascular necrosis of femoral head. In: Ganesh RN, editor. *Applied biological engineering—principles and practice*. Rijeka: InTech. p 347–364.
10. Mavčič B, Iglič A, Kralj-Iglič V, et al. 2008. Cumulative hip contact stress predicts osteoarthritis in DDH. Clin Orthop 466:884–891.
11. Pompe B, Daniel M, Sochor M, et al. 2003. Gradient of contact stress in normal and dysplastic human hips. Med Eng Phys 25:379–385.
12. Mavčič B, Pompe B, Antolič V, et al. 2002. Mathematical estimation of stress distribution in normal and dysplastic human hips. J Orthop Res 20:1025–1030.
13. Zupanc O, Krizančič M, Daniel M, et al. 2008. Shear stress in epiphyseal growth plate is a risk factor for slipped capital femoral epiphysis. J Pediatr Orthop 28:444–451.
14. Daniel M, Dolinar D, Herman S, et al. 2006. Contact stress in hips with osteonecrosis of the femoral head. Clin Orthop 447:92–99.
15. Rečnik G, Kralj-Iglič V, Iglič A, et al. 2009. The role of obesity, biomechanical constitution of the pelvis and contact joint stress in progression of hip osteoarthritis. Osteoarthritis Cartilage 17:879–882.
16. Rečnik G, Kralj-Iglič V, Iglič A, et al. 2007. Higher peak contact hip stress predetermines the side of hip involved in idiopathic osteoarthritis. Clin Biomech 22:1119–1124.
17. Iglič A, Antolič V, Srakar F. 1993. Biomechanical analysis of various operative hip joint rotation center shifts. Arch Orthop Trauma Surg 112:124–126.
18. Herman S, Jaklič A, Herman S, et al. 2002. Hip stress reduction after Chiari osteotomy. Med Biol Eng Comput 40:369–375.
19. Dolinar D, Antolič V, Herman S, et al. 2003. Influence of contact hip stress on the outcome of surgical treatment of

hips affected by avascular necrosis. Arch Orthop Trauma Surg 123:509–513.
20. Mavčič B, Slivnik T, Antolič V, et al. 2004. High contact hip stress is related to the development of hip pathology with increasing age. Clin Biomech 19:939–943.
21. Brand RA, Iglič A, Kralj-Iglič V. 2001. Contact stresses in human hip: implications for disease and treatment. Hip Int 11:117–126.
22. Catterall A. 1971. The natural history of Perthes' disease. J Bone Joint Surg Br 53-B:37–53.
23. Herring JA, Neustadt JB, Williams JJ, et al. 1992. The lateral pillar classification of Legg-Calve-Perthes disease. J Pediatr Orthop 12:143–150.
24. Stulberg SD, Cooperman DR, Wallensten R. 1981. The natural history of Legg-Calvé-Perthes disease. J Bone Joint Surg Am 63-A:1095–1108.
25. Kellgren JH, Lawrence JS. 1957. Radiological assessment of osteo-arthrosis. Ann Rheum Dis 16:494–502.
26. Harris WH. 1969. Traumatic arthritis of the hip after dislocation and acetabular fractures: treatment by mold arthroplasty. An end-result study using a new method of result evaluation. J Bone Joint Surg Am 51:737–755.
27. Bellamy N, Buchanan WW, Goldsmith CH, et al. 1988. Validation study of WOMAC: a health status instrument for measuring clinically important patient relevant outcomes to antirheumatic drug therapy in patients with osteoarthritis of the hip or knee. J Rheumatol 15:1833–1840.
28. Mahadeva D, Chong M, Langton DJ, et al. 2010. Reliability and reproducibility of classification systems for Legg-Calvé-Perthes disease: a systematic review of the literature. Acta Orthop Belg 76:48–57.
29. Brinckmann P, Frobin W, Hierholzer E. 1981. Stress on the articular surface of the hip joint in healthy adults and persons with idiopathic osteoarthrosis of the hip joint. J Biomech 14:149–153.
30. Shah H, Siddesh ND, Pai H, et al. 2013. Quantitative measures for evaluating the radiographic outcome of Legg-Calvé-Perthes disease. J Bone Joint Surg 95:354–361.
31. Herring JA, Kim HT, Browne R. 2004. Legg-Calve-Perthes disease. Part I: classification of radiographs with use of the modified lateral pillar and Stulberg classifications. J Bone Joint Surg Am 86:2103–2120.
32. Wiig O, Terjesen T, Svenningsen S. 2007. Inter-observer reliability of the Stulberg classification in the assessment of Perthes disease. J Child Orthop 1:101–105.
33. Park MS, Chung CY, Lee KM, et al. 2012. Reliability and stability of three common classifications for Legg-Calvé-Perthes disease. Clin Orthop 470:2376–2382.
34. Guille JT, Lipton GE, Tsirikos AI, et al. 2002. Bilateral Legg-Calve-Perthes disease: presentation and outcome. J Pediatr Orthop 22:458–463.
35. Kersnič B, Iglič A, Kralj-Iglič V, et al. 1997. Increased incidence of arthrosis in female population could be related to femoral and pelvic shape. Arch Orthop Trauma Surg 116:345–347.
36. Aaron RK, Voisinet A, Racine J, et al. 2011. Corticosteroid-associated avascular necrosis: dose relationships and early diagnosis. Ann N Y Acad Sci 1240:38–46.
37. Duthie RB. 1996. Arthritis and rheumatic diseases. In: Duthie RB, Bentley G, editors. *Mercer's orthopaedic surgery*, 9th ed. London: Arnold; p 751–857.
38. Jones LC, Mont MA, Le TB, et al. 2003. Procoagulants and osteonecrosis. J Rheumatol 30:783–791.
39. Gürkan E, Yildiz I, Oçal F. 2006. Avascular necrosis of the femoral head as the first manifestation of acute lymphoblastic leukemia. Leuk Lymphoma 47:365–367.
40. Lawson-Ayayi S, Bonnet F, Bernardin E, et al. 2005. Avascular necrosis in HIV-infected patients: a case-control study from the Aquitaine Cohort 1997–2002. Clin Infect Dis 40:1188–1193.
41. Kang PD, Shen B, Yang J, et al. 2007. Platelet and endothelial cell-derived microparticles in steroid-induced osteonecrosis of the femoral head of rabbit model. Chung-Hua Hsueh Tsa Chih 87:2045–2049.
42. Ogura H, Kawasaki T, Tanaka H, et al. 2001. Activated platelets enhance microparticle formation and platelet-leukocyte interaction in severe trauma and sepsis. J Trauma 50:801–809.
43. Mallat Z, Benamer H, Hugel B, et al. 2000. Elevated levels of shed membrane with procoagulant potential in the peripheral circulating blood of patients with acute coronary syndrome. Circulation 101:841–843.
44. Oyabu C, Morinobu A, Sugiyama D, et al. 2011. Plasma platelet-derived microparticles in patients with connective tissue diseases. J Rheumatol 38:590–592.
45. Blum A. 2009. The possible role of red blood cell microvesicles in atherosclerosis. Eur J Intern Med 20:101–105.
46. Ogasawara F, Fusegawa H, Haruki Y, et al. 2005. Platelet activation in patients with alcoholic liver disease. Tokai J Exp Clin Med 30:41–48.
47. Hulkova H, Poupetova H, Harzer K, et al. 2010. Abnormal nonstoring capillary endothelium: a novel feature of Gaucher disease. Ultrastructural study of dermal capillaries. J Inherit Metab Dis 33:69–78.
48. Lynch SF, Ludlam CA. 2007. Plasma microparticles and vascular disorders. Br J Haematol 137:36–48.
49. Larsson A, Lundahl T, Eriksson M, et al. 1996. Endotoxin induced platelet microvesicle formation measured by flow cytometry. Platelets 7:153–158.
50. Savasan S, Buyukavci M, Buck S, et al. 2004. Leukaemia/lymphoma cell microparticles in childhood mature B cell neoplasms. J Clin Pathol 57:651–653.
51. Kadiu I, Narayanasamy P, Dash PK, et al. 2012. Biochemical and biologic characterization of exosomes and microvesicles as facilitators of HIV-1 infection in macrophages. J Immunol 189:744–754.
52. Janša R, Šuštar V, Frank M, et al. 2008. Number of microvesicles in peripheral blood and ability of plasma to induce adhesion between phospholipid membranes in 19 patients with gastrointestinal diseases. Blood Cells Mol Dis 41:124–132.
53. Muller I, Klocke A, Alex M, et al. 2003. Intravascular tissue factor initiates coagulation via circulating microvesicles and platelets. FASEB J 17:476–478.
54. Šuštar V, Bedina Zavec A, Štukelj R, et al. 2011. Nanoparticles isolated from blood—a reflection of vesiculability of blood cells during the isolation process. Int J Nanomed 6:2737–2748.
55. Kim YJ, Novais E. 2011. Diagnosis and treatment of femoroacetabular impingement in Legg-Calve´-Perthes disease. J Pediatr Orthop 31:235–240.
56. Eijer H, Podeszwa DA, Ganz R, et al. 2006. Evaluation and treatment of young adults with femoro-acetabular impingement secondary to Perthes' disease. Hip Int 16:273–280.
57. Ganz R, Parvizi J, Beck M, et al. 2003. Femoroacetabular impingement: a cause for osteoarthritis of the hip. Clin Orthop Relat Res 417:112–120.
58. Leunig M, Beaule PE, Ganz R. 2009. The concept of femoroacetabular impingement: current status and future perspectives. Clin Orthop Relat Res 467:616–622.